FLOMEKO 2003
11th IMEKO TC9 Conference on Flow Measurement
Groningen, NETHERLANDS, 12 - 14 May 2003

NUMERICAL SIMULATIONS OF THE FLUID FLOW IN THE MEASURING TUBE OF THE CORIOLIS FLOWMETER

Gregor Bobovnik, Jože Kutin, Ivan Bajsic

University of Ljubljana, Faculty of Mechanical Engineering, Laboratory of Measurements in Process Engineering, Ljubljana, Slovenia

The flow of a viscous fluid through a straight measuring tube of a coriolis flowmeter was investigated using numerical simulations. Numerical simulations were performed by the Comet code, which is based on the finite volume method. The simulations were made for various Reynolds numbers at several vibrating frequencies of the measuring tube. The evolution of the axial velocity, a distortion of the axial velocity profiles, a secondary flow in the measuring tube, and a twisting moment acting on the tube's wall were observed. Values of the twisting moment that acts around the centre of the tube's length were used to evaluate the performance of the flowmeter at different mass flow rates and various dimensions of the measuring tube.

1 INTRODUCTION

In a coriolis flowmeter, a fluid-conveying measuring tube maintained vibrating at its natural frequency, is used as a primary sensing element. Variations of the measuring tube's natural frequency and the mode shape deflection are used for measurements of a fluid density and a mass flow rate, respectively.

The inlet velocity profiles that result from the various installation positions are in general one of the most crucial influences on the performance of the flowmeters. But there were very few attempts made to determine the effects of different inlet-flow conditions on the characteristic of the coriolis mass flowmeter. Hemp [1] used the weight vector theory to study the influence of the velocity profiles on a simple configuration of the coriolis flowmeter, consisting of an unsupported straight tube unattached to the adjacent piping. These results show that the sensitivity of the flowmeter is higher for turbulent than for laminar flow when the end effects are taken into account.

Durst and Raszillier [2] analytically determined fully developed laminar flow in a tube, rotating about an axis perpendicular to its own. A presence of the secondary flow, which occurs in the rotating tube, is also expected in the vibrating measuring tube of the coriolis flowmeter. The authors suggested that this might be an additional source of the tube's anti-symmetrical deformation.

The transient developing laminar flow in a tube oscillating around the vertical diameter at its entrance was studied numerically in [3]. It was established that the initial conditions (oscillation pattern of the tube) influence the transient regime but have no significant effect on the flow field once the periodic regime (steady-state) is reached. A different model configuration does not allow the results to be directly implemented for the measuring tube of the coriolis flowmeter.

In this paper we used results of numerical simulations to investigate the velocity field in the vibrating tube and possible effects of different flow conditions on the performance of the flowmeter. Numerical simulations performed using the Comet code [4] were used to investigate the velocity and pressure field in the vibrating measuring tube. The evolution of the axial velocity profiles in the measuring tube, a presence of the secondary flow, and the pressure field were of special interest. It is important to emphasize that the strain-stress analysis of the measuring tube (solid) was not included in the numerical model, therefore the vibrational shape of the tube was prescribed in each

time step of the simulation process. The twisting moment acting around the centre of the tube's length was calculated from the pressure field and was used for estimation of the anti-symmetrical coriolis effect, which is exploited as the basic principle for the mass flow measurements. The paper begins with the presentation of the velocity field in the rotating tube [2] that served as a starting point in the analysis of the flow in the vibrating tube.

2 LAMINAR FLOW IN A ROTATING TUBE

Durst and Raszillier [2] studied the incompressible laminar flow in a tube that rotates about an axis perpendicular to its own with constant angular velocity Ω (Fig. 1).

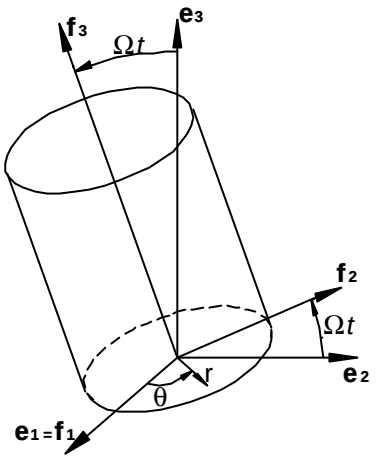

Fig. 1. Rotating tube

We can represent the stationary velocity field in the tube in a form of perturbation series, based on the assumption that the drop of viscous pressure is constant along the tube axis and that the velocity field is identical in each cross-section of the tube. Axial velocity v and stream function Ψ, representing the transversal velocity field, and radial position r can be written in terms of corresponding dimensionless quantities w, ψ, x:

$$\begin{aligned} v(r,\theta) &= \frac{\nu}{R} w(x,\theta), \\ \Psi(r,\theta) &= \nu\psi(x,\theta), \\ r &= Rx, \end{aligned} \tag{1}$$

where R represents the tube radius and ν the kinematic viscosity of the fluid. The solutions for w and ψ are written as:

$$\begin{aligned} w(x,\theta) &= \sum_{n=0}^{\infty} Ta^n w_n(x,\theta), \\ \psi(x,\theta) &= \sum_{n=0}^{\infty} Ta^n \psi_n(x,\theta), \end{aligned} \tag{2}$$

where Ta is the Taylor number

$$Ta = \frac{2\Omega R^2}{\nu}. \tag{3}$$

The first terms (n = 0) of the solution in (2) represent the Hagen-Poiseuille flow

$$w_0(x,\theta) = c\left(1-x^2\right) \text{ in } \psi_0(x,\theta) = 0\,, \tag{4}$$

where *c* defines a parameter characterizing the flow velocity and is in the case of the Hagen-Poiseuille flow precisely equal to the Reynolds number, *Re*, [2].

Higher orders represent the perturbation of the Hagen-Poiseuille flow produced by the rotation of the tube. First and second order perturbations in (2) have the following form:

$$\psi_1(x,\theta) = \frac{c}{3\cdot 2^5}\, x\left(1-x^2\right)^2 \cos\theta\,, \tag{5}$$

$$w_1(x,\theta) = \frac{c^2}{3^2\cdot 2^8}\, x\left(1-x^2\right)\left(x^4-3x^2+3\right)\sin\theta\,, \tag{6}$$

$$\psi_2(x,\theta) = \frac{c^2}{5\cdot 3^3\cdot 2^{15}}\, x^2\left(1-x^2\right)^2\left(17-2x^2-x^4\right)\sin 2\theta\,, \tag{7}$$

$$\begin{aligned} w_2(x,\theta) = {} & \frac{c}{2^7\cdot 3^2}\left(x^2-1\right)^3 + \frac{c^3}{2^{17}\cdot 3^4\cdot 5}\left(x^2-1\right)^4\left(-10x^4+32x^2-37\right) + \\ & + \frac{c}{2^9\cdot 3^2}\, x^2\left(x^2-1\right)\left(3x^2-5\right)\cos 2\theta + \\ & + \frac{c^3}{2^{17}\cdot 3^4\cdot 5^2\cdot 7}\, x^2\left(x^2-1\right)\left(48x^8-302x^6+958x^4-1457x^2+923\right)\cos 2\theta\,. \end{aligned} \tag{8}$$

The axial and the secondary velocity field obtained from the above given solutions are presented in Fig. 2.

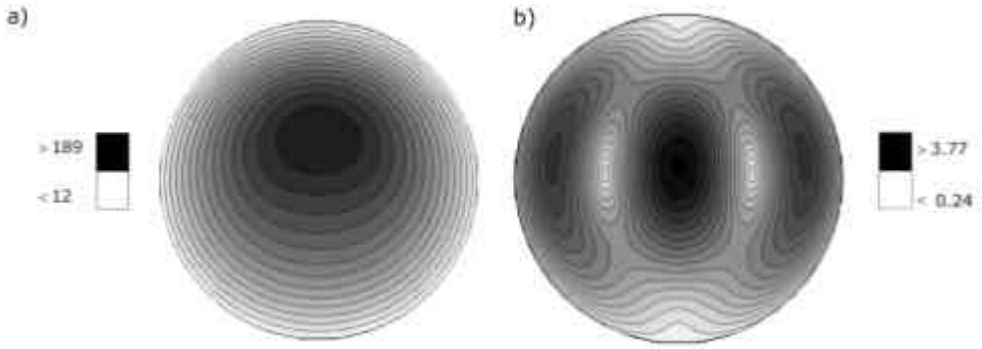

Fig. 2. a) Axial, *w,* and b) transversal (secondary), ψ, velocity field for *c* = 200 and *Ta* = 2.

A total force that acts on a fluid particle with volume Φ in a rotating frame is generally written as a sum of the coriolis, the centripetal and the tangential inertial force, respectively [5]:

$$\mathbf{F} = -\int_{\Phi} 2\rho(\mathbf{O}\times\mathbf{v})\,d\Phi - \int_{\Phi}\rho\left(\mathbf{O}\times(\mathbf{O}\times\mathbf{r})\right)d\Phi - \int_{\Phi}\rho\left(\frac{d\mathbf{O}}{dt}\times\mathbf{r}\right)d\Phi\,, \tag{9}$$

where **v** is the relative velocity of the fluid.

The tangential force is, in the case of a constant angular velocity, equal to 0. In this case, the coriolis force is the one that has a significant influence on the velocity field in the tube. It causes the region of the highest axial velocities in the cross-section to move closer to the tube's trailing edge, which triggers the secondary fluid motion in the transversal plane of the tube, as presented in Fig. 2.

Observing the flow in the vibrating tube, all three fluid forces in (9) become important. The influence that certain force will have on the resulting velocity field depends on the tube's vibrating frequency, *f*, on the through-flow Reynolds number and on the dimensions of the measuring tube as it will be presented later in the text. The flow in the measuring tube of the coriolis flowmeter, which usually vibrates at relatively high frequencies, will be probably strongest influenced by the tangential inertial force.

3 NUMERICAL MODEL

Numerical simulations were performed by the Comet code that uses finite volume discretization method. The flow of the viscous fluid through the tube was modelled as isothermal and incompressible. This section presents the mathematical model that was incorporated in the program, the geometry of the computational domain and the initial and boundary conditions of the simulations.

3.1 Mathematical model

The basic equations used for fluid flow description in the Comet are presented in this section. The equations are presented for isothermal fluid flow, so the energy equation is not included in the model. For the fluid with density ρ, velocity vector **v** and surface velocity (of the finite volume) $\mathbf{v}_s$ the continuity and the momentum equations are stated as:

$$\frac{\partial}{\partial t}\int_{\Phi}\rho \mathrm{d}\Phi + \int_{S}\rho\left(\mathbf{v}-\mathbf{v}_s\right)\mathrm{d}\mathbf{s} = 0 \tag{10}$$

and

$$\frac{\partial}{\partial t}\int_{\Phi}\rho\mathbf{v}\mathrm{d}\Phi + \int_{S}\rho\mathbf{v}\left(\mathbf{v}-\mathbf{v}_s\right)\cdot\mathrm{d}\mathbf{s} = \int_{S}\mathbf{T}\cdot\mathrm{d}\,\mathbf{s} + \int_{\Phi}\mathbf{f}_b\mathrm{d}\Phi\,, \tag{11}$$

where $\mathbf{f}_b$ represents the vector of forces acting on the fluid volume Φ and **T** the strain tensor defined as:

$$\mathbf{T} = 2\mu_e\,\mathbf{D} - \frac{2}{3}\mu_e\,\mathrm{div}\,\mathbf{v}\,\mathbf{I} - \left(p + \frac{2}{3}\left(\mu_t\,\mathrm{div}\,\mathbf{v} + \rho k\right)\right)\mathbf{I}\,, \tag{12}$$

where

$$\mathbf{D} = \frac{1}{2}\left(\mathrm{grad}\,\mathbf{v} + \left(\mathrm{grad}\,\mathbf{v}\right)^T\right) \tag{13}$$

is the rate of strain tensor, *p* is the pressure, **I** is the unit tensor and μ_e is the effective viscosity of the fluid defined as the sum of the dynamic μ and the turbulent μ_t viscosity:

$$\mu_e = \mu + \mu_t \tag{14}$$

The turbulent viscosity is obtained using the standard *k*-ε model that needs two additional transport equations to be solved. Turbulence was not included in the simulations, where the through-flow Reynolds number was lower than 1000.

3.2 Computational domain

The computational domain consists of the measuring tube, and the inlet and outlet sections, the dimensions of which (with respect to the inner diameter of the tube, *D = 2R*) are presented in Fig. 3. Only the fluid flow in the measuring tube was of our interest, however the inlet and outlet

sections were included in the model to minimize the disturbances that were introduced in the flow by the vibration of the measuring tube. Simulations were made for three different dimensions of the measuring tube. The inner diameter of the tube was equal to 0.03, 0.02 and 0.015 m, respectively. The length of the measuring tube was constant (L = 0.3 m), so the ratios L/D were equal to 10, 15 and 20, respectively. The axial velocity profiles were observed in cross-sections O, T_1, T_2, I, the positions of which are also shown in Fig. 3.

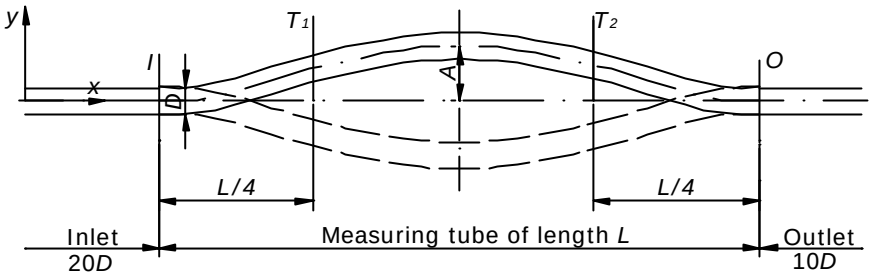

Fig. 3. Scheme of the computational domain

The numerical grids used in the simulations consisted, with respect to the chosen ratios L/D of 77140, 94240 and 112100 cells (finite volumes), respectively. The cells representing the measuring tube were uniformly distributed in the axial direction, while the distances between the centres of the cells in the inlet (outlet) region were increased by factor 1.03 towards the beginning (end). The number of the cells in the cross-section was equal to 380.

3.3 Boundary and initial conditions

The fluid (computational) domain changed its shape in each time step, according to the first mode shape of a clamped-clamped beam [6]:

$$\begin{aligned} w_1(x,t) &= C_1 F_1(x)\cos(\omega t) \\ &= C_1\left[\cosh\left(\lambda_1\frac{x}{L}\right)-\cos\left(\lambda_1\frac{x}{L}\right)-\frac{\cosh\lambda_1-\cos\lambda_1}{\sinh\lambda_1-\sin\lambda_1}\left(\sinh\left(\lambda_1\frac{x}{L}\right)-\sin\left(\lambda_1\frac{x}{L}\right)\right)\right]\cos(\omega t), \end{aligned} \tag{15}$$

where λ_1 is the coefficient that determines the first mode shape and C_1 is the factor that defines the amplitude of the vibration and $\omega = 2\pi f$ is the circular frequency of the tube (f is the vibrating frequency of the tube). In case of the first mode shape λ_1 = 4.730 and $C_1 = A/F_1(L/2)$ and A defines the amplitude of vibration in the middle of the tube, which is in our case $L/300$.

Fully developed velocity profiles were prescribed at the inlet boundary and were obtained from the preliminary simulations of the flow in a tube (of length $45D$) at rest. In case of the turbulent flows, the values of the turbulent energy and its dissipation rate, which were obtained from preliminary simulations, were also introduced on the inlet. The vibration of the tube started when the flow of the fluid reaches its stationary state. A single oscillation period of the tube was modelled with 130 time steps. The simulations were performed for the range of Reynolds numbers from 400 to 100000, using the tube vibrating frequencies between 10 and 300 Hz.

4 RESULTS

4.1 Evolution of the velocity profile

The evolution of the axial velocity and also the pressure was observed to determine when the periodic regime (in the reminder of the text named as steady-state) in the tube was reached.

In Fig. 4, the evolution of the axial velocity is presented for the tube vibration frequency 10 Hz in the middle of cross-sections *O*, T_1, T_2, *I*. It takes app. 4 periods (0.4 s) for the amplitudes of the velocity oscillations to become constant (steady-state). The oscillations around the average value in the centre of the cross-sections are relatively small (± 0.02%). Larger oscillations are expected near the tube's wall, because of the asymmetrical velocity profile distortions as shown in the next sections. It was established that the duration of the transient regime lengthens with higher Reynolds numbers and lower vibrating frequencies. In most simulations the steady-state was reached after 2 or 3 periods.

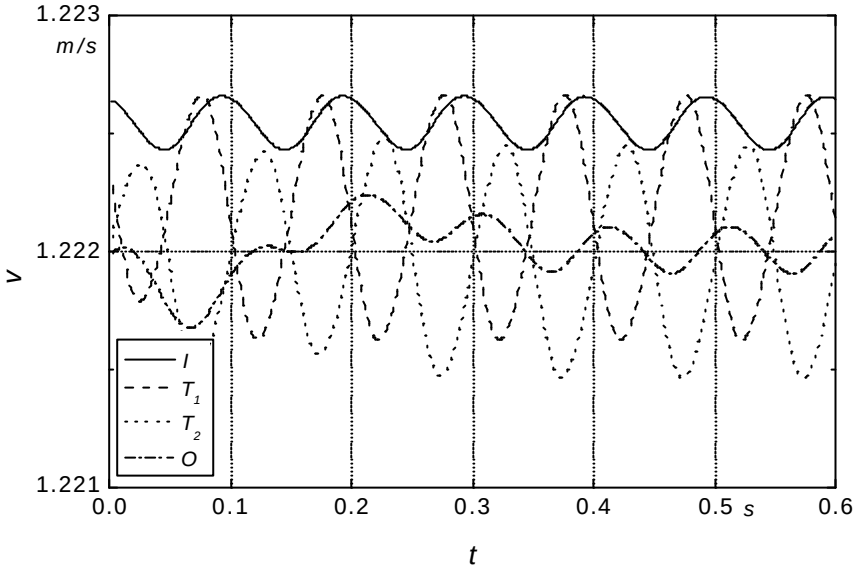

Fig. 4. Evolution of axial velocity in the middle of cross-sections *O*, T_1, T_2, *I* for *Re* = 20000, f = 10 Hz and *L*/*D* = 15

4.2 Axial velocity profiles

Axial velocity profiles were observed in cross-sections *O*, T_1, T_2 and *I* in the middle position of the measuring tube - $\cos(\omega t) = 0$. In Fig. 5, the axial velocity profiles are presented for *Re* = 4000 and *f* = 100 Hz (variable *V* represents the average axial velocity). The velocity profiles in the inlet (*I*) and outlet (*O*) sections of the measuring tube are practically identical as the fully developed velocity profile for the selected *Re*, which shows that the disturbances caused by vibration are not transmitted far away from the measuring tube. The velocity profiles in cross-sections T_1 and T_2 show asymmetry with respect to each other and have the maximum velocities higher than the fully developed profile. The maximum axial velocity in cross-section T_1 is increased by 3.5 % (with respect to the fully developed velocity profile) and is positioned on $r/R \approx 0.35$.

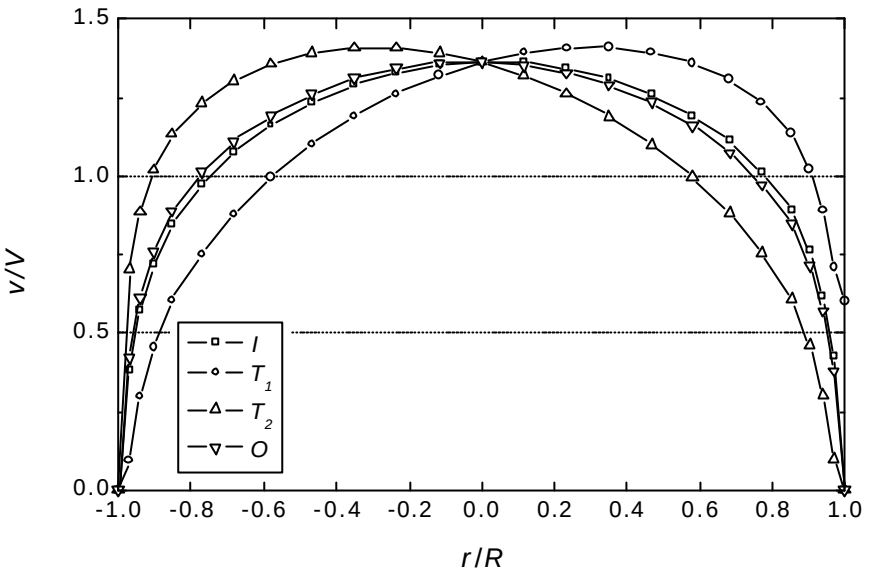

Fig. 5. The axial velocity profiles in cross-sections O, T_1, T_2 and I for Re = 4000, f = 100 Hz and L/D = 15

Fig. 6 presents the influence of different vibrating frequencies on the axial velocity profiles in cross-section T_1. It is evident that the distortion of the velocity profile depends on the vibrating frequency of the tube. The largest axial velocity in the cross-section and the most obvious profile distortion are observed at the highest vibrating frequency f = 300 Hz. The transition of the maximum velocities in the profiles towards the inner wall of the tube triggers the secondary flow. In Fig. 7, the secondary flow field is schematically presented. The magnitudes of the secondary flows are up to 300-times smaller (for Re = 20000 and f = 10 Hz) than the average axial velocity.

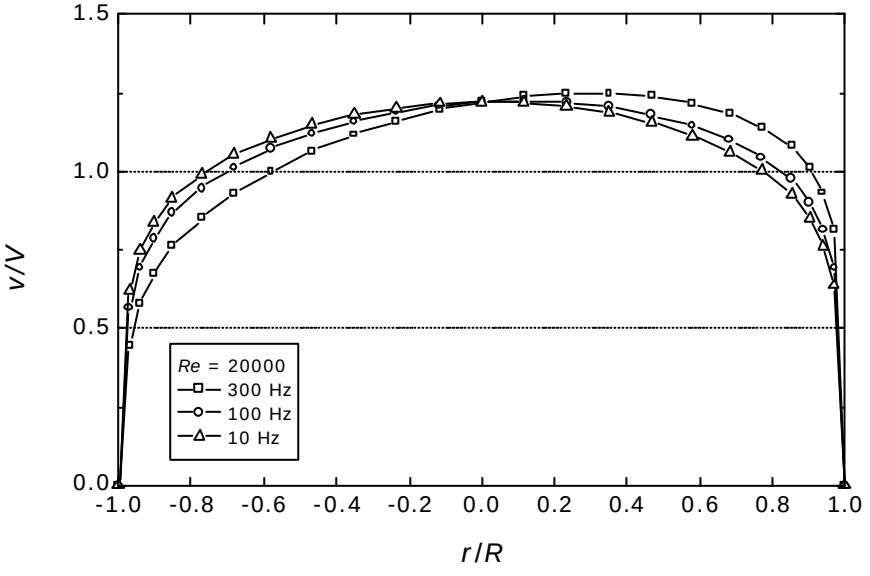

Fig. 6. The axial profile distortion in cross-section T_1 at constant Re with respect to the vibrating frequency (L/D = 15)

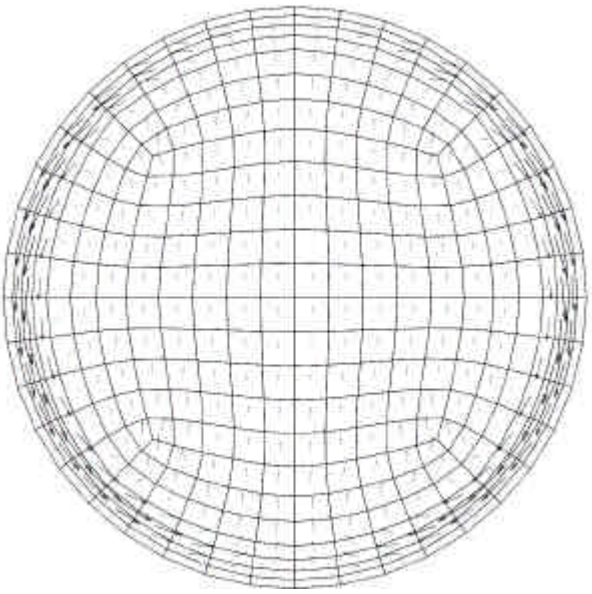

Fig. 7. Schematic presentation of the secondary flow in cross-section T_1

In cross-section T_1, the velocity profile was observed during one half of the tube's oscillation period as presented in Fig. 8. The tube is moving upwards (the direction of the motion is shown in Fig. 8), starting at its lowest position, where $\cos(\omega t) = -1$. In the lowest position of the tube, the axial velocity profile is very similar to the fully developed profile. The angular velocity is, in this position of the tube, equal to 0, therefore the flow of the fluid experiences only the translational and the tangential inertial forces, the magnitudes of which decrease, when the tube approaches its middle position. When the tube travels into its middle position, where $\cos(\omega t) = 0$, the maximum velocities in the profiles start moving towards the leading edge of the tube. The maximum distortion of the velocity profile is reached almost exactly in the tube's middle position. In the tube's middle position the coriolis and the centrifugal inertial forces act on the fluid in the transversal direction. In cross-section T_1, the coriolis force acts on the flow in the opposite direction of the tube motion, so the distortion of the velocity profile cannot simply be explained by the coriolis effect. Analysing the resulting velocity field, it was established that the tangential force introduced swirls in opposite directions in both halves of the tube in x-y plane, which caused the observed profile distortion. As the tube travels from its middle into its upper position, where $\cos(\omega t) = 1$, the profiles distortion diminishes, because the tangential force changes its direction. The velocity profile in the upper position of the tube is almost identical to that in the lower position of the tube. The flow conditions in cross-section T_2 are exactly contrary to those observed in cross-section T_1.

From the observations presented in this section, it is clear that the velocity field in the measuring tube of the coriolis mass flowmeter is not influenced by the coriolis force as strongly as in the case of the tube rotating with the constant angular velocity. The tangential inertial force, which results from a local angular acceleration, causes the deflection of the velocity profile as presented in Fig. 5 to Fig. 8. For high vibrating frequencies, large amplitudes of the vibration and small through-flow Reynolds numbers even a flow reversal is expected near the trailing edge of the tube. The effect of the coriolis force is expected to be greater in the region of lower vibrating frequencies.

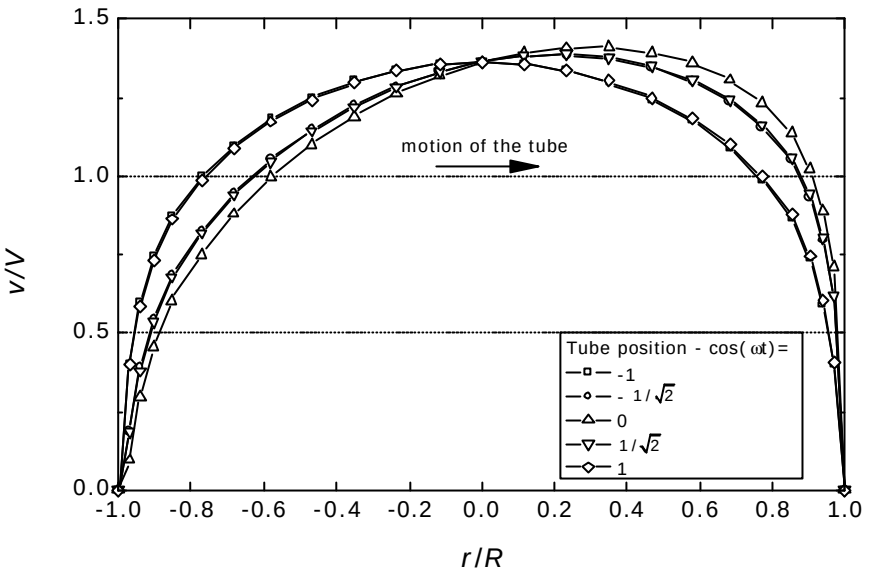

Fig. 8. Evolution of the axial velocity profile during the tube's oscillation in cross-section T_1 (Re = 4000, f = 100 Hz and L/D = 15)

4.3 The twisting moment

A deflection of the tube's mode shape is used as the basic measuring principle in the coriolis mass flowmeter. Because the strain-stress analysis of the tube was not performed, the value of the twisting moment, which results from the anti-symmetric fluid force distribution, is used to evaluate the performance of the flowmeter at various Reynolds numbers and vibrating frequencies of the tube. The value of the moment, which acts around the centre of the tube's length, is calculated in the middle position of the tube, where the "anti-symmetric" coriolis force reaches its magnitude.

By taking into account the measuring tube that is dived into N equally wide rings along its length L, the value of the moment M is calculated as (Fig. 9):

$$M = \sum_{j=1}^{N} F_{j,y} \left(\frac{L}{2} - \left(j - \frac{1}{2} \right) \cdot \frac{L}{N} \right), \tag{16}$$

where the $F_{j,y}$ represents the fluid force that acts in the centre of a particular ring in the y-direction:

$$F_{j,y} = \sum_{k \in j} F_{k,y} \ . \tag{17}$$

$F_{k,y}$ is the force acting on the boundary element k of the ring j and is calculated from the pressure field obtained from the simulations. In general it is the sum of the frictional $T_{k,y}$ and the pressure forces $p_k s_{k,y}$, where $s_{k,y}$ is the component y of the surface vector of the boundary k:

$$F_{k,y} = T_{k,y} + p_k s_{k,y} \ . \tag{18}$$

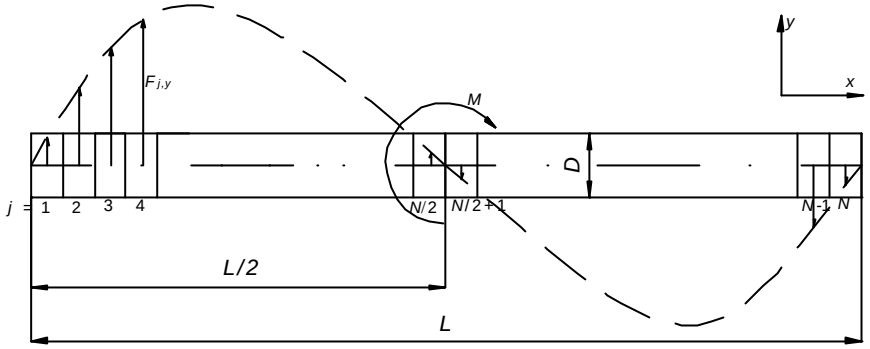

Fig. 9. Calculation of the twisting moment

Reducing the moment value from (16) by the mass flow rate q_m, the vibrating frequency f, the amplitude of the vibration in the middle of the tube A, and the length of the tube L, we get a dimensionless value of the twisting moment M_n:

$$M_n = \frac{M}{q_m f A L} . \tag{19}$$

Assuming a one-dimensional flow, the dimensionless value of the moment remains constant for any values of the parameters in the denominator of (19) and is equal to:

$$M_n^* = 6.57428 . \tag{20}$$

The flowmeter performance was estimated with the ratio M_n / M_n^*, where the value M_n is obtained from the results of the numerical simulations. The value of this ratio tells us how far the computed values agree with the one-dimensional fluid-flow model and knowing that the flowmeter characteristic is linear, in case of the one-dimensional fluid-flow assumption, a deviation of numerical results from linear characteristic of the mass flowmeter is established.

The ratios of M_n / M_n^* for various vibrating frequencies of the measuring tube are presented in Fig. 10. It is clear that the numerical results are in good agreement with the assumption of the one-dimensional flow and that the vibrating frequency does not influence the value of the ratio and thereby the characteristic of the flowmeter. It is also observed that the ratio is smaller for lower values of the Reynolds numbers, meaning, that the characteristic of a coriolis flowmeter is not completely linear in this region – the sensitivity of the flowmeter decreases.

We performed additional simulations at different ratios L/D to determine the effect of the measuring tube's dimensions on the characteristic of the flowmeter. The results are presented in Fig. 11. As expected, the ratio M_n / M_n^* is closest to 1 for the measuring tube, with the length 20-times longer than its diameter. For all dimensions the ratio changes in a similar manner, so it is clear that the deviation of the linear characteristic of the flowmeter at low Reynolds numbers is not related to the dimensions (aspect ratio L/D) of the measuring tube, although a higher sensitivity decrease is expected for the measuring tube with L/D = 10.

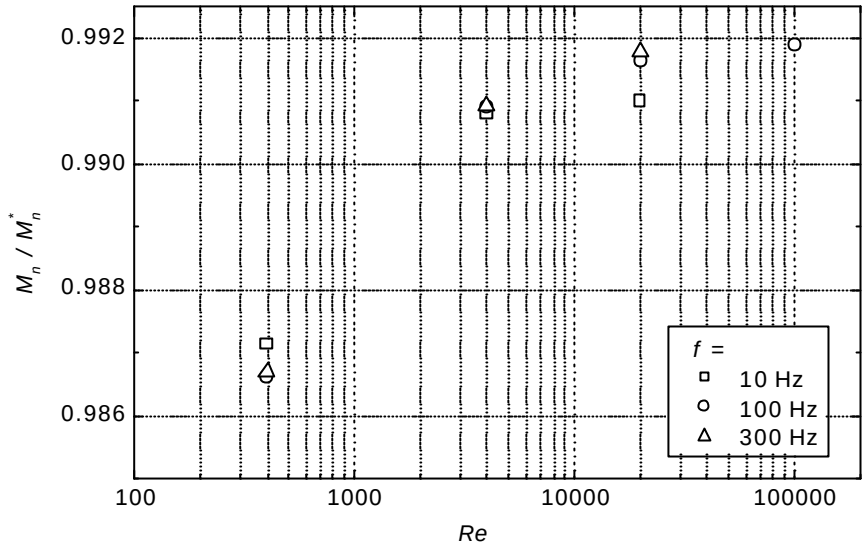

Fig. 10. Ratio M_n / M_n^* for various vibrating frequencies of the measuring tube (L/D = 15)

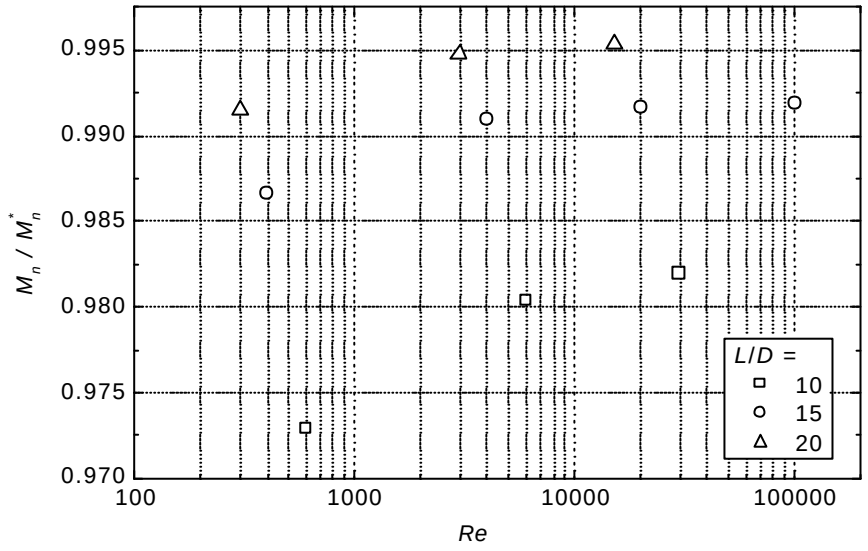

Fig. 11. Ratio M_n / M_n^* for various dimensions of the measuring tube (f = 100 Hz)

5 CONCLUSIONS

The flow of a viscous fluid through the measuring tube of a coriolis mass flowmeter was observed using the results of the numerical simulations. The tangential inertial force has the strongest influence on the velocity field inside the measuring tube and causes asymmetrical distortions of the velocity field in the opposite halves of the measuring tube. A higher impact of the coriolis force is expected for lower vibrating frequencies of the tube and for higher through-flow Reynolds numbers.

Further, the possible effects of various through-flow Reynolds numbers on the characteristic of the flowmeter were investigated, using the value of the twisting moment, which resulted from the pressure field obtained from the simulation results. The results show that a decrease of the

sensitivity is expected in the lower range of Reynolds numbers, with a higher sensitivity decrease for the measuring tubes with lower ratios L/D.

6 REFERENCES

[1] J. Hemp, Calculation of the sensitivity of a straight tube coriolis mass flowmeter with free ends, Flow Measurement and Instrumentation, vol. 12(5-6), pp. 411 – 420, 2002.

[2] F. Durst, H. Raszillier, Flow in a rotating straight pipe, with view on coriolis mass flow meter, Journal of Fluids Engineering, vol. 112, pp. 149 – 154, 1990.

[3] B. Benhamou, N. Galanis, A. Laneville, Transient effects of orthogonal pipe oscillations on laminar developing incompressible flow, International Journal for Numerical Methods in Fluids, vol. (34), pp. 561 – 584, 2001.

[4] Comet version 2.00 – user manual, Institute of Computational Continuum Mechanics GmbH (ICCM), Hamburg, 2001.

[5] T. D. Burton, Introduction to dynamic system analysis, McGraw-Hill, Inc., 1994.

[6] R. D. Blevins, Formulas for natural frequency and mode shape, Krieger, Malabar, 1995.